

DENSITY THRESHOLDS IN AND EFFICIENCIES OF STAR FORMATION

ANDREAS BURKERT^{1,2} AND LEE HARTMANN³

Submitted to ApJ

ABSTRACT

Recent studies by Lada et al. (2010) and Heiderman et al. (2010) have suggested that efficient star formation occurs above an approximate threshold in gas surface density Σ of $\Sigma_c \sim 120 M_\odot \text{pc}^{-3}$ ($A_K \sim 0.8$). We find no precise threshold for star formation; the impression of such results from a continuous and steep power-law increase of the ratio of protostellar mass to molecular gas mass with Σ , approaching unity at protostellar core densities, corresponding to $\Sigma \sim 1000 M_\odot \text{pc}^{-3}$. We argue that this increase in star formation efficiency results from the increasing importance of self-gravity with increasing density, along with the consequent decrease in evolutionary timescales. The observations are consistent with models in which regions of more diffuse molecular gas with column densities corresponding to $A_V \sim 1 - 2$ are initially formed by converging galactic hydrodynamic flows which subsequently collapse gravitationally, producing a power-law relation between surface density and the area A spanned at that density of $A \sim \Sigma^{-3.2}$. We show that the finding of a strong correlation between the amount of gas above Σ_c and the young stellar population by Lada et al. (2010) with ratios q of dense gas mass to stellar mass of $8 \gtrsim q \gtrsim 3$ requires *continuing* formation of dense gas, also consistent with the idea of gravitational collapse. Finally, we note that the suggested linear relationship between the star formation rate and molecular gas mass at very high surface densities in galactic studies arises as a result of probing small size and high density scales where rapid gravitational collapse is occurring and the efficiency of star formation approaches unity.

Subject headings: ISM: clouds, ISM: structure, stars: formation

1. INTRODUCTION

Local star formation has long been known to be strongly enhanced in the densest regions of molecular clouds (e.g., Lada 1992; Lada et al. 1993; Mizuno et al. 1995; Onishi et al. 1998; Johnstone et al. 2004). The increasingly large and sensitive surveys of molecular clouds using a variety of techniques have now made it possible to derive more quantitative relationships between star formation and dense gas. In particular, using measurements of infrared extinction, Lada et al. (2010, L10) and Heiderman et al. (2010, H10) proposed that galactic star formation is strongly enhanced above a critical gas surface density corresponding to $\Sigma_c \sim 120 M_\odot \text{pc}^{-2}$, approximately the same threshold Onishi et al. (1998) derived from C¹⁸O observations of the Taurus molecular cloud. In addition, H10 and Lada et al. (2010, 2012) inferred that star formation rates (SFRs) depend approximately linearly on the amount of molecular gas above the threshold, qualitatively consistent with findings from extragalactic studies (Gao & Solomon 2004; Bigiel et al. 2011), although with differing normalizations.

In this paper we suggest that there is no precise threshold for star formation, but densities must be high enough so that the self-gravity of the gas is important. We show that the observations are consistent with a continuous progression of the increasing importance of gravity and decreasing evolutionary timescales with increasing

density. We argue that the observations of L10 generally require *continuing* formation of dense gas, as predicted by models of molecular clouds undergoing large-scale gravitational collapse (e.g., Hartmann et al. 2001; Vázquez-Semadeni et al. 2007; Heitsch et al. 2007, 2008; Heitsch & Hartmann 2008; Zamora-Avilés et al. 2012). We point out that the relation between the star formation rate (SFR) per unit area and the surface density found by H10 only becomes linear at very high surface densities where the efficiency of star formation is very large; we suggest that this results in a linear relation between the star formation rate and Σ , particularly when density-sensitive tracers are used. Finally, we show that the data of H10 suggest that at high densities clouds exhibit a similar power-law dependence of the area A at a given surface density Σ , $A(\Sigma) \propto \Sigma^{-3.2}$, which might provide important constraints for theories of the structure of molecular clouds.

2. OBSERVATIONAL EVIDENCE FOR THRESHOLDS

It is useful to first review the observational constraints in some detail. We begin by considering the findings of L10 who examined the ratio of the gas mass above a given level of extinction (or surface density) M_g to the number of young stars N in several nearby star-forming regions. They searched for the value of Σ which would most nearly result in a linear relation between M_g and N for the various clouds; the resulting critical value was found to be $\Sigma_c = 116 \pm 25 M_\odot \text{pc}^{-2}$. While L10 identified this as a threshold for star formation, they did note that there was a factor of nearly two in Σ for which the dispersion in M_g/N among the various clouds was minimal.

To examine further the evidence for a threshold surface density, we consider the findings of H10. These authors established roughly equally-spaced contour levels of (in-

burkert@usm.lmu.de, lhartm@umich.edu

¹ University Observatory Munich, Scheinerstrasse 1, D-81679 Munich, Germany

² Max-Planck-Fellow, Max-Planck-Institute for Extraterrestrial Physics, Giessenbachstrasse 1, 85758 Garching, Germany

³ Department of Astronomy, University of Michigan, 830 Denison, 500 Church St., Ann Arbor, MI 48109-1042, USA

frared) extinction in a sample of low-mass star-forming regions, and then measured both the area and the number of protostellar (Class I and flat-spectrum) sources contained within each extinction or surface density contour. By focusing upon objects thought to be protostars, and thus a) very young and b) still accreting from their natal envelopes, H10 tried to minimize the conceptual difficulties which arise because the gas one observes at the present epoch is *not* the gas that produced the stars.

The left panel of Figure 1 shows the main results of H10 for the low-mass star-forming regions. We plot this as the number of young stars N per unit contour area A vs. Σ ; this is equivalent to the star formation rate of H10, which is simply N/A multiplied by an average protostellar mass and divided by a (constant) timescale of 2 Myr. (We have added together the Class I and flat-spectrum sources to improve the small number statistics; see discussion in the Appendix.) The ratio N/A is steeply dependent upon the molecular gas surface density, increasing by about three orders of magnitude over a range of about one order of magnitude in Σ , qualitatively consistent with the idea of a threshold, although there is no sign of a transition in the N/A vs. Σ relation at their suggested threshold of $\Sigma_c = 129 \pm 14 M_\odot \text{pc}^{-2}$ (dotted vertical line in Figure 1).

In the Appendix we discuss the findings of H10 in more detail. Here we note that the correlation between N/A and Σ is mostly driven by the correlation between the area A of the contours as a function of Σ , where $A \propto \Sigma^{-3.2}$. Thus, the order of magnitude range in Σ probed in Figure 1 corresponds to a range of three orders of magnitude in A ; moving to higher values of surface density implies restricting attention to ever-decreasing areas and volumes. In addition, if N is independent of Σ , N/A increases by three orders of magnitudes, consistent with the trend, shown in the left panel of Figure 1.

In fact, the relevant physical quantity for star formation is more likely to be the volume density ρ than Σ . If we make the guess, as discussed further in the Appendix, that the typical length scale along the line of sight at Σ is $l \sim A^{1/2}$, the range of one order of magnitude in Σ spanned in Figure 1 corresponds to a range of roughly a factor of 300 in ρ and a decrease by a factor of 17 in collapse timescale. It is therefore not surprising that the number of young stars per unit area, or the star formation rate per unit area as in H10, is a rapidly increasing function of Σ (see discussion in §3).

The impression of a threshold for star formation is enhanced in H10 by their inclusion of an additional data set spanning higher surface densities than present in their study of low-mass regions. Including data from massive clumps with surface densities measured from HCN and star formation rates SFR estimated from infrared luminosities L_{IR} from Wu et al. (2010), H10 find a more nearly linear relationship between the SFR and Σ , spanning the range from $300 \lesssim \Sigma/M_\odot \text{pc}^{-2} \lesssim 3000$. The intersection of this linear branch with the low-mass star formation branch, discussed above and shown in Figure 1, lies at about $\Sigma_c = 120 M_\odot \text{pc}^{-2}$ which H10 interpret as a signature of a threshold. However, as H10 acknowledge, there are concerns about combining results using two different methodologies, from two very different types of regions (low-mass star-forming regions vs. massive cores

with $L_{IR} > 10^{4.5} L_\odot$ and thus forming massive stars) (see also §5). First of all, the physics of high-mass star formation might differ from low-mass star formation. Secondly, the results from the low-mass regions do not identify a particular value of Σ_c but instead extend smoothly into regions with $\Sigma > \Sigma_c$. As a result, the linear branch of high-mass star forming clumps does not start where the low-mass star formation branch ends. It instead intersects the low-mass branch somewhere as one would expect if both branches are two independent correlations with different slopes. In this case, the surface density Σ_c at the point of intersection has no physical meaning and cannot be interpreted as a threshold above which star formation depends linearly on gas surface density with a steeper dependence below this threshold.

Assuming for the moment that high-mass star formation proceeds in a similar way as low-mass star formation, how can we then reconcile the linear behavior of the high-mass star formation branch with the strongly non-linear relationship, observed for the low-mass star forming regions? The linear, high-mass star formation branch traces gas with molecular core densities of $\geq 10^5 \text{cm}^{-3}$. To examine the implications for low-mass star formation we examine the star-gas correlation at these high densities. In the right panel of Figure 1 we show the ratio of protostellar masses to the mass of gas within the contour at Σ^4 . At high surface densities the “efficiency” of star formation, as measured by the ratio of dense gas mass to protostellar mass, exceeds 0.1 and reaches values of order unity at molecular core surface densities of $\Sigma \sim 1000 M_\odot \text{pc}^{-2}$. At this point the non-linear increase of stellar mass versus dense gas mass with surface density is expected to break down as it is unlikely that more than 50% of a core turns into stars. If there exists a maximum or typical efficiency for dense cores to form stars one would therefore naturally expect to observe a transition towards a linear N/A vs. Σ relation above a critical value of M_*/M_g . As suggested in the Appendix, if in the massive cores the HCN tends to trace these particular, dense environments and thus also a particular dynamical collapse time, a linear relation between the gas mass and star formation rate might ensue.

One should also note that the area spanned at the highest observed surface densities is of order $A \sim 10^{-1} \text{pc}^2$ (see Appendix). This implies that the length scales probed at the highest values of Σ are $\sim A^{1/2} \sim 0.3 \text{pc}$. The H10 data is averaged over 270 arcsec beams, which at the typical distances of the studied clouds of $\sim 150 - 300 \text{pc}$ corresponds to resolutions of $0.2 - 0.4 \text{pc}$. Thus dense, low-mass protostellar cores with typical sizes of 0.1pc (Myers & Benson 1983), will drop out of the high- Σ region; cores that are surrounded by much lower density material will then appear at lower- Σ . This again emphasizes the conceptual difficulties involved in relating the (extended) gas seen at the current epoch to the gas that formed (or is most directly forming) the observed stars.

3. “THRESHOLDS” VS. CONTINUOUS EVOLUTION

3.1. Overview

⁴ We caution that this plot shows intrinsically correlated parameters, as the gas mass is derived by multiplying the area of the contour by Σ , so the slope of the relation is not significant.

As shown in the previous section, while H10 find a rapid increase in the SFR or N/A over a region in surface densities that includes the suggested threshold surface density, there is no obvious break in the relation, precisely at Σ_c . Still the rapid increase of M_*/M_g for surface densities that lie within a factor of 3-4 around Σ_c could be interpreted as a threshold for efficient star formation. Consistent with these results, here we argue that apparent thresholds like this occur in continuously-evolving clouds because: most molecular clouds form at modest densities and pressures; the gas must become much more dense on its way to form a star; the evolutionary (gravitational collapse) timescales rapidly become shorter as the gas becomes denser; and therefore the contrast of low-density, slow evolution vs. high-density, fast evolution leads to the impression of a threshold.

Consider an estimate of the central pressure of a gas cloud $P = P_{ex} + \pi G \Sigma^2 / 2$, where P_{ex} is the external gas pressure and Σ is the surface or column density (Elmegreen & Elmegreen 1978). This relation holds exactly for an infinite hydrostatic sheet and is roughly correct for many other geometries. Now, at the suggested critical surface density of $\Sigma_c \sim 120 M_\odot \text{pc}^{-2}$, $P \sim 100 \times P_{ex}$ if we assume a typical local interstellar medium (ISM) pressure $P_{ex}/k \sim 10^4 \text{cm}^{-3} \text{K}$.

To achieve such ram pressures from flows at 10km s^{-1} , typical of the turbulent ISM velocity dispersions in regular star-forming galaxies (Dib et al. 2006), would require very large external flow densities of $\gtrsim 35 \text{cm}^{-3}$. In addition, to produce a region of this extinction, corresponding to hydrogen column density of $N_H \sim 1.4 \times 10^{22} \text{cm}^{-2}$, would require the converging or expanding flows to last for a timescale

$$\tau = \frac{\Sigma}{2v_\infty n_\infty} = 1.1 \times 10^8 \text{yr} \left(\frac{10 \text{km s}^{-1}}{v_\infty} \right) \left(\frac{2 \text{cm}^{-3}}{n_\infty} \right), \quad (1)$$

which is a factor of ten to twenty times larger than expected from large-scale numerical simulations of the dynamics of the turbulent ISM in disk galaxies (Dobbs et al. 2012) that indicate cloud formation timescales of order $5 \times 10^6 - 10^7$ yrs; again, one would require initial densities of $20 - 40 \text{cm}^{-3}$ to build the cloud in reasonable timescales.

Most of the mass of molecular (CO) clouds in the solar neighborhood lies at column densities corresponding to $A_V \sim 1 - 2$ (e.g., Goldsmith et al. 2008); i.e., there is an extended, lower-density molecular envelope surrounding the dense, strongly self-gravitating gas, which would be at best slowly contracting due to its self gravity (see below). At $A_V \sim 2$, or a surface density $\sim 40 M_\odot \text{pc}^{-2}$, the pressure due to self gravity would be $P/k \gtrsim 6 \times 10^4 \text{cm}^{-3} \text{K}$, only about an order of magnitude larger than the typical ISM pressure. This is indeed a natural result of forming molecular clouds (at least in the solar neighborhood) by interstellar medium (ISM) flows with densities of \gtrsim a few cm^{-3} at velocities of order 10km s^{-1} , as simulated by (Ballesteros-Paredes et al. 1999; Audit & Hennebelle 2005; Hennebelle & Audit 2007; Vázquez-Semadeni et al. 2007; Heitsch et al. 2008; Heitsch & Hartmann 2008). Moreover, such surface densities *can* be formed in the requisite timescales, especially if the inflowing material has slightly higher densities than

that of the average ISM (Dobbs et al. 2012).

Thus, while the majority of gas in molecular clouds is at (relatively) low densities, and can be produced by external ISM ram pressures, gas at or above Σ_c is very likely to be generated and bound mainly by gravity. Independent support for this argument comes from analyses of the probability density functions (Npdf; the equivalent of the $A(\Sigma)$ relations discussed in §2 and in the Appendix) of the column densities of molecular clouds (Kainulainen et al. 2009, 2011; Froebrich & Rowles 2010). The Npdfs appear lognormal at low densities, which is generally interpreted as the result of turbulence-dominated flows (Vázquez-Semadeni 1994; Ostriker et al. 2001), but they exhibit power-law tails at high column densities in star-forming clouds, as do the results of H10 (§2, Appendix). Ballesteros-Paredes et al. (2011) showed that such power-law tails naturally arise when gravitationally-driven motion becomes more important than pure hydrodynamic turbulence, consistent with our picture.

Note that although H10 find a rapid increase in star formation efficiency of about three orders of magnitude near Σ_c , it actually takes place over a range of one order of magnitude in Σ which corresponds to two orders of magnitude in “self-gravity pressure”. Moreover, we argued previously that this range in Σ corresponds to a factor of ~ 300 in volume density; this corresponds to a decrease in the free-fall time $\propto \rho^{-1/2}$ of more than one order of magnitude at high densities. Thus the combination of strong self-gravity and rapid evolution will enhance the impression of a threshold.

3.2. Self-gravitating sheet simulation

To illustrate our argument in a more graphical way, we use some simple numerical simulations. We consider a massive sheet of gas which could have arisen as a result of colliding flows as in the simulations of Vázquez-Semadeni et al. (2007); Heitsch et al. (2008); Heitsch & Hartmann (2008). We ignore turbulent motions and assume that the cloud is initially completely quiescent but generates supersonic velocities via global and local gravitational collapse. The setup is basically the same as that used in Burkert & Hartmann (2004), where we considered a uniform circular sheet.

The sheet is in hydrostatic equilibrium and in pressure equilibrium with a constant surrounding pressure of $P/k = 5 \times 10^4 \text{K cm}^{-3}$. The initial conditions are the radius R of the sheet, its mass M , and the sound speed c_s of the gas. We assume an isothermal equation of state with the pressure $P = c_s^2 \rho$. Here, we took an initial cloud radius of $R = 10 \text{pc}$, a sound speed of $c_s = 0.2 \text{km s}^{-1}$ and calculated results for initial sheet masses ranging from $M_c = 10^3 M_\odot$ to $2 \times 10^4 M_\odot$. The calculations were performed with the SPH code outlined by Bate & Burkert (1997) and Burkert & Alves (2009).

Figure 2 shows the surface density of our standard model with $M_c = 10^3 M_\odot$ at two times. With the adopted initial conditions, a dense ring develops near the edge of the cloud, due to highly non-linear accelerations of gravity (e.g., Burkert & Hartmann 2004). In effect, we have made a circular and in this case artificially smooth, dense filament, situated within a lower-density cloud. The ring/filament continues to grow as the cloud (which

has many Jeans masses) globally contracts, accumulating mass and becoming denser as time proceeds.

Figure 3 (left) shows the evolution of the mean ring volume densities for the standard model (solid line) as well as for additional models with differing initial masses and thus surface densities. The density evolution can be characterized by two phases, “slow” and “fast”, a distinction which is clearest for the two lowest-mass models. The upper limit to the “slow” timescale is the collapse time t_{coll} for the sheet as a whole (Burkert & Hartmann 2004),

$$t_{coll} \approx \left(\frac{R}{\pi G \Sigma} \right)^{1/2} \sim (G \langle \rho \rangle)^{-1/2}. \quad (2)$$

In other words, t_{coll} is the global free-fall time of the sheet characterized by $\langle \rho \rangle$, the mean density over the spherical volume enclosed by R . Equation (2) yields a global collapse time of 15 Myr for $M_c = 10^3 M_\odot$. In this case the sheet contracts considerably before the ring (filament) density runs away. Because the sheet volume density scales as Σ^2 , the timescale for collapse of the ring becomes much faster with increasing surface density.

Figure 3 demonstrates our basic explanation of apparent thresholds for star formation. The timescales over which the cloud remains at low column densities are one to a few Myr, consistent with the global sheet collapse timescale. The surface density in the ring at first grows slowly as it is initially pressure supported. At some point however enough material has been accumulated and the ring becomes gravitationally unstable. It collapses onto itself, leading to runaway growth in density that is much faster than the growth in mean density in the sheet and resulting in two gas phases, a diffuse gaseous component and an embedded dense collapsing filament that now can fragment and form stars. The collapse occurs essentially at the free-fall time of the *local* density, very similar to the evolution under pure free-fall that is shown in the right panel of Figure 3. The two timescales of the collapsing ring and of the diffuse sheet are comparable to observational estimates of cloud lifetimes (Hartmann et al. 2001) and protostellar/starless core lifetimes (Evans et al. 2009), respectively.

Of course these simulations are also highly unrealistic, in that clouds will have multiple sites of star formation; but one might view Figures 2 and 3 as representing the evolution of differing parts of the cloud or even differing local patches, with the same basic result. Indeed, even the limiting case of the uniform pressureless sphere collapse exhibits the aspect of slow initial growth and localised fast runaway collapse.

Note that in our simulations, the entire cloud is gravitationally bound and collapsing. However, even if we do not support the low-density medium via e.g. turbulence or magnetic fields, a broad range of evolutionary timescales develops due to ring formation (see also Pon et al. 2011).

4. EFFICIENCY OF STAR FORMATION ABOVE Σ_C

L10 argue that the total number of young stars, or the stellar mass M_* , is much better correlated with the mass of dense gas M_g above the threshold Σ_c than with the total gas mass in the star-forming region. To explore this further, in Figure 4 we plot the data from Table 2

of L10 in the form of the ratio of the dense gas mass to stellar mass $M_g/M_* = q$, vs. the ratio of the total gas mass M_{tot} to M_g , again using an average mass per star of $0.7 M_\odot$. Discounting the Lupus 4 region for poor stellar counting statistics, and noting that the stellar population of Orion B may be underestimated due to high extinction and nebulosity (S.T. Megeath, personal communication), the data suggest that the least-active regions with large values of q have low fractions of dense gas, while in the most active regions the fraction of dense gas is high, which may be an indication of cloud evolution. For the most active and probably evolved star-forming regions, (apart from Orion B) there is a relatively modest range in the gas to stellar mass of $8 \gtrsim q \gtrsim 3$.

An important implication can be derived from these results. As all the young stars have not formed at the same time (indeed, some of them are still-accreting protostars), M_* must be increasing with time; therefore the mass of dense gas M_g *must also increase in time* to keep q above unity and within a modest range. Thus, the L10 results imply that star-forming clouds are not in a quasi-static state but are continuing to evolve (Dobbs et al. 2011a,b, 2012).

To illustrate further implications of the data, we consider a simple analytic model. Let us assume that a dense molecular gas component is generated at a rate \dot{M}_{in} . Suppose also that a fraction ϵ of the dense gas turns into stars on its local free-fall timescale τ_{ff}

$$\frac{dM_g}{dt} = \dot{M}_{in} - \frac{dM_*}{dt}, \quad (3)$$

$$\frac{dM_*}{dt} = \frac{\epsilon}{\tau_{ff}} M_g, \quad (4)$$

where we take ϵ and τ_{ff} to be constants. Typical values of ϵ are $\epsilon \approx 0.1$ (L10). Let us first demand that at any given time t the ratio $q = M_g/M_*$ is constant. We then find

$$M_g(t) = M_{g,0} \exp(t/t_0), \quad (5)$$

where $M_{g,0} = M_g(t=0)$ is the initial dense gas mass when star formation starts and t_0 is the exponential growth timescale of the dense gas mass,

$$t_0 = \frac{\tau_{ff}}{q\epsilon}. \quad (6)$$

Inserting equation (5) into equation (3) we find

$$\dot{M}_{in} = \epsilon(q+1) \frac{M_{g,0}}{\tau_{ff}} \exp\left(\frac{t}{t_0}\right) \quad (7)$$

Thus, if q were absolutely constant, there would need to be an *exponential infall and increase of dense gas mass with time*.

This exponential growth model raises some concerns. First of all, obviously M_g cannot increase exponentially forever. In addition, as the fraction of dense gas is observed to be always small compared to the diffuse gas mass and as the efficiency of star formation is generally only a few percent of the total cloud mass (e.g., Evans et al. 2009; Krumholz et al. 2012), exponential growth would imply a very delicate timing for dispersal of the whole cloud. Stellar feedback would have

to destroy the cloud before a large fraction of its diffuse gas has been converted to dense gas. Finally, it is not clear that simulations provide support for continued exponential growth of the dense gas mass (e.g., Vázquez-Semadeni et al. 2009, see §3.2). To address this problem we develop a second analytic model which assumes linear rather than exponential growth in the dense gas mass with time. Adopting time units $\tau = t/\tau_{ff}$ and assuming a constant \dot{M}_{in} , the solutions of equations (3) and (4) now are

$$M_g(\tau) = M_{g,0} e^{-\epsilon\tau} + \dot{M}_{in} \tau_{ff} (1 - e^{-\epsilon\tau})/\epsilon, \quad (8)$$

$$M_*(\tau) = M_{g,0}(\tau = 0) (1 - e^{-\epsilon\tau}) + \dot{M}_{in} \tau_{ff} [\tau - (1 - e^{-\epsilon\tau})/\epsilon]. \quad (9)$$

Figure 5 shows results, assuming $M_{g,0} = 0$ for efficiencies of 0.1 and 0.3, respectively. For values of $\epsilon \approx 0.1$ that are consistent with the observations of T10, q remains in the observed range over $4\tau_{ff}$.

L10 suggested that the critical surface density might correspond to a critical *volume* density $n_c = 10^4 \text{ cm}^{-3}$, implying $\tau_{ff} \sim 0.35$ Myr. Thus, with linear growth of the dense gas mass, Figure 5 indicates that even for star formation efficiencies of $\epsilon = 0.1$, the observed range of q can only be maintained for less than 1-1.5 Myr, considerably shorter than typical estimates of star-forming cloud lifetimes which are of order $2 - 4 \times 10^6$ yrs. However, there are reasons to question this estimate of the critical volume density. In the Appendix we use the data of H10 to examine the issue further, by estimating the path length along the line of sight to be $l \sim A^{1/2}$ and thus $\langle \rho \rangle \sim \Sigma/A^{1/2}$. While the results differ from cloud to cloud, we find a narrow range of estimated mean densities at Σ_c between $n_c \sim 500 \text{ cm}^{-3}$ and $\sim 2.6 \times 10^3 \text{ cm}^{-3}$. Taking a mean value for all clouds of $n_c \sim 10^3 \text{ cm}^{-3}$ implies a free-fall time of ~ 1 Myr. This makes it much easier to explain the range of q found by L10 as q now would lie in the observed regime for 4×10^6 yrs which are reasonable star formation timescales of molecular clouds. As a consistency check, the areas at Σ_c of one to several pc^2 are much larger than those typical of low mass pre-stellar cores of densities of 10^4 cm^{-3} (e.g., Myers & Benson 1983).

We can also use the numerical simulations to check the arguments constraining q . The left-hand panel in Figure 6 shows the growth of mass with densities above 10^3 cm^{-3} for the standard model. One observes that the growth of dense gas is exponential for the first ~ 0.2 Myr, but then becomes roughly linear. If we were to keep q strictly constant, the cloud would have to be dispersed at the end of the short epoch of exponential growth which is not in agreement with observed star formation timescales. To illustrate the implications further, in the right panel of Figure 6 we show $q = M_g/M_*$ as a function of time for the standard model with M_* the mass in the circular filament above $n(H_2) = 10^3 \text{ cm}^{-3}$, but at a free-fall time of 1 Myr earlier, times an efficiency factor ϵ . In other words, here we assume again that ϵM_g turns into stars after one free fall timescale. The dotted curve assumes $\epsilon = 1$, the solid red curve $\epsilon = 0.3$, and the dashed curve $\epsilon = 0.1$.

Figure 6 reinforces the analytic results. For efficien-

cies of order 10% q will lie in the range found by L10 for 4 free fall timescales. If, in addition, the free fall timescale is of order 1 Myr, as expected for critical densities of $n(H_2) = 10^3 \text{ cm}^{-3}$, q would remain in the observed regime for the typical lifetimes of star-forming regions. The pure analytic model actually does a good job of reproducing these combined numerical-“post processing” results in Figure 6 (for example, it predicts that for $\epsilon = 0.1$, q drops below ~ 3 at $4\tau_{ff} \sim 4$ Myr).

Dense gas formation is probably not monolithic, but instead is the result of differing regions collapsing at differing times. The blue solid curve, labeled *I*, shows the situation if we assume that after every $\tau_{ff} = 1$ Myr a new, independent dense gas region forms that does exactly the same thing as the $\epsilon = 0.3$ case, just starting later. So e.g. after 2 Myr we have in total 3 star forming regions: one is 2 Myr old, one is 1 Myr old and just beginning to form stars, and one is just starting to generate dense gas but is not forming stars yet. This spreading of the onset of star formation is helpful but does not change the main result.

Finally, the behavior of q implies something about the efficiency of turning gas into stars. Sometimes star formation sites are characterized by the “star formation efficiency per free-fall time” $\eta_{ff} = SFR \times \tau_{ff}/M_g$ (Krumholz et al. 2012). Considering only the gas mass above Σ_c , L10 find a low value $\eta_{ff} \approx 0.02$; however, this depends upon their assumption of $n_c = 10^4 \text{ cm}^{-4}$. If instead $n_c = 10^3 \text{ cm}^{-4}$, then $\eta_{ff} \sim 0.06$.

The concept of η_{ff} is complicated, not only because real clouds exhibit a wide range of densities and thus regions with very different free-fall timescales, but also because it depends upon the assumption of a quasi-steady state. For example, if the gas mass grows exponentially as in the model which provides strictly constant q ,

$$\eta_{ff} = (qt/\tau_{ff})^{-1}. \quad (10)$$

Note that η_{ff} , despite its name, does not depend explicitly on the star formation efficiency ϵ , that is the fraction of dense gas that turns into stars in τ_{ff} . A low value of η_{ff} is therefore not in conflict with theoretical models that would predict higher values of ϵ . Given q , η_{ff} is instead a measure of the lifetime t of the star forming region in units of its free fall time that is being continuously fed by infall from its diffuse molecular envelope. Even if the growth is not strictly exponential, there is still a tendency to underestimate η_{ff} , as well as significant uncertainty as to what the conditions were in the past when the first stars formed Vázquez-Semadeni et al. (e.g., 2009).

5. DISCUSSION AND CONCLUSIONS

We have shown that the observations of H10 and L10 do not require precise density thresholds for star formation; all that is required is rapid gravitational collapse at high densities coupled with the presence of a much lower-density molecular cloud formed via plausible interstellar medium flows. This “external” low-density molecular material feeds the dense regions. The low-density gas can also be gravitationally collapsing and still provide a more slowly-evolving structure with more mass than in the dense regions, especially if the global cloud geometry is far from spherical. If the flows into the dense regions

are driven by gravitational acceleration, the increase of dense gas mass with time to keep the ratio of dense gas to stars relatively constant naturally occurs. The resulting picture is consistent with simulations of dynamically-evolving, gravitationally-collapsing star-forming molecular clouds. Density diagnostics are needed to help translate surface densities into volume densities, which then will constrain the free-fall times and thus the efficiencies of star formation at modest surface densities.

The data of H10 suggest that, at high Σ , the efficiency of converting the mass of gas into stars appears to approach unity; we suggest that the linear relationship between SFR and Σ then arises because this dense gas is already in gravitational collapse. The survival of this linear relationship in extragalactic, beam-diluted observations suggests an approximate common scaling of the mass of dense gas with gas mass above Σ_c ; an open question is whether this is a result, or can be derived from, the apparent “power-law” distribution of areas as a function of density. The origin of the $A(\Sigma)$ relation is unclear and has to be related to the universal density structure of clouds; the transition between the log-normal form of the Npdf at low column densities to the power law behavior seen in studies of star formation by H10 and others is likely the product of gravitational collapse (Ballesteros-Paredes et al. 2011).

Along the way we have noted some of the conceptual difficulties in deriving density thresholds for and efficiencies of star formation. The dense gas we see at the present epoch is not the gas that formed, or is forming the young stars currently present. Can we then assume a steady state to interpret the observations and linking past star formation to present cloud structure? In the case of galactic molecular clouds, we have argued that one in general cannot assume such a steady state. Beyond this, will the gas that we see at any density at the current epoch turn into stars later? Yet another conceptual problem is what volume(s) should one choose to examine in order to determine a threshold for or efficiency of making stars. In the picture we have presented here, with continuous evolution of lower-density gas into high-density, star-forming gas, it is not obvious how one would choose any particular scale. As stars can *only* be formed from gas that has much higher densities than that of the interstellar medium in general, it is not clear what one learns from connecting young stars with the very densest gas. Extragalactic observations over large scales may sidestep these questions to some extent by averaging over sufficient volumes that steady states may be achieved; but then the question is whether physical insight is suppressed by such global averaging. A fuller understanding of star formation must involve the cycling of gas between low- and high-density phases.

This work was supported in part by NSF grant AST-0807305. AB acknowledges useful conversations with Mark Krumholz and Clare Dobbs, LH with Javier Ballesteros-Paredes.

6. APPENDIX

Here we look a little more closely at the data which go into producing the H10 results illustrated in Figure 1, using the data from their Tables 1 and 2.

While the N/A vs. Σ relation appears well-defined, it is in fact more of a reflection of the behavior of A vs. Σ than of the protostars. This can be seen in the left panel of Figure 7 which shows a weak correlation between the number of protostars in a contour at a given Σ . The correlation shown in Figure 1 is driven by the area in a specific contour A vs. Σ behavior, which is shown in the right panel of Figure 7. Of course protostars are formed necessarily by high-density gas; the lack of correlation in the left panel is probably mostly a result of small number statistics; even at high Σ , there exist regions with no embedded protostar (downward-pointing triangles in Figure 7). In addition, one can see evidence for correlations between N and Σ for individual regions with reasonable stellar statistics (for example, Oph, Cha, and Ser-Aql; see Figure 1 for symbol identification). Nevertheless, the slope of N/A vs. Σ is basically determined by the slope of the $A(\Sigma)$ relation.

It is clear from the right panel of Figure 7 that a large fraction of the scatter in the $A(\Sigma)$ relation is due to the superposition of different regions (coded by different symbols), each of which having intrinsically similar slopes but differing offsets. This leads to the plausible conjecture that more massive clouds have larger areas at a given surface density, leading to correspondingly more stars per Σ bin. To investigate this possibility, in Figure 8 we plot the area divided by a scaled total mass from Table 1 of H10. The result is a greatly reduced scatter around the trend line.

Formally, the least-squares fit using the errors from H10 and eliminating the Ser-Aql region for the unscaled data in Figure 7 yields

$$\log A(\text{pc}^2) = (-3.58 \pm 0.21) \log(\Sigma/120\text{M}_\odot \text{pc}^{-2}) + 0.56 \pm 0.05. \quad (11)$$

while for the scaled data of Figure 8 it is

$$\log A(\text{pc}^2)/M_{\text{tot}}(2000\text{M}_\odot) = (-3.24 \pm 0.18) \log(\Sigma/120\text{M}_\odot \text{pc}^{-2}) + 0.62 \pm 0.05. \quad (12)$$

Here we have chosen to normalize at the approximate surface density “threshold” $\Sigma_c = 120\text{M}_\odot\text{pc}^{-2}$ of L10 and H10.⁵ The power-law behavior $A \sim \Sigma^{-3.2}$ is reasonably consistent with that observed in studies of the probability density function of column density (e.g., Kainulainen et al. 2009; Froebrich & Rowles 2010), although Froebrich & Rowles (2010) suggest that the slope may vary depending upon spatial resolution.

This analysis of $A(\Sigma)$ leads to another important issue; specifically, the important physical variable is the local *volume* density ρ , not Σ . There is no unique way to convert a surface density to a volume density distribution without using density diagnostics. However, it is instructive to make the following guess. We suppose that the area projected upon the sky A at a given value of Σ is representative of that which would be seen from an orthogonal projection, at least on average. In other words, we assume that the characteristic average scale

⁵ This is *not* the Larson (1981) scaling relation, $\rho \propto r^{-1.1}$, which would imply $\Sigma \approx \text{constant}$ (see discussion in Ballesteros-Paredes et al. 2012)

length along the line of sight is $h \sim A^{1/2}$; thus

$$\rho \sim \Sigma/A^{1/2}. \quad (13)$$

Using equation 12, the value of the critical surface density area is $A(\Sigma_c) \sim 4\text{pc}^2(M_{tot}/2000M_\odot)$; this implies a median length scale for $M_{tot} \approx 2000M_\odot$ of $h \sim 2$ pc. For $\Sigma_c = 120M_\odot \text{pc}^{-2} = 2.5 \times 10^{-2} \text{gcm}^{-2}$, or a column density $N(H_2) = 6.3 \times 10^{21} \text{cm}^{-2}$, the average volume density is then $n(H_2) = 10^3 \text{cm}^{-3}(M_{tot}/2000M_\odot)^{-0.5}$. We might go further and use the mass range in M_{tot} explored by H10 to estimate upper and lower ranges. This results in estimate densities at Σ_c of $n(H_2) \sim 500 \text{cm}^{-3}$ and $\sim 2.6 \times 10^3 \text{cm}^{-3}$ respectively. This is important to keep in mind when evaluating models which explain the observations of q (§4).

This analysis of the $A(\Sigma)$ relation leads to another important point; in proceeding to higher values of Σ , H10 is probing *smaller volumes*. Indeed, applying the fit obtained for the median dependence of $A(\Sigma)$ (equation 12), at $\Sigma \sim 1000M_\odot \text{pc}^{-2}$ the typical length scale being probed is $h \sim 0.1$ pc and thus the implied average volume density is $n(H_2) \sim 10^5 \text{cm}^{-2}$, essentially protostellar core volumes and densities.

This interpretation of the linear SFR vs. Σ relation as simply observing gas which is forming stars at maximum efficiency is further supported by the fact that the use of infrared luminosity to determine the SFR for the HCN clumps by Wu et al. (2010) is only possible as reasonably massive stars have *already* formed in these regions. If by using HCN a specific density range is being identified, and thus a specific free-fall time, a linear relation between the star formation rate and gas mass follows.

REFERENCES

- Audit, E., & Hennebelle, P. 2005, A&A, 433, 1
 Ballesteros-Paredes, J., Hartmann, L., & Vázquez-Semadeni, E. 1999, ApJ, 527, 285
 Ballesteros-Paredes, J., Vázquez-Semadeni, E., Gazol, A., et al. 2011, MNRAS, 416, 1436
 Ballesteros-Paredes, J., D'Alessio, P., Hartmann, L., MNRAS, in press
 Bate, M. R., & Burkert, A. 1997, MNRAS, 288, 1060
 Bigiel, F., Leroy, A. K., Walter, F., et al. 2011, ApJ, 730, L1
 Burkert, A., & Alves, J. 2009, ApJ, 695, 1308
 Burkert, A., & Hartmann, L. 2004, ApJ, 616, 288
 Dib, S., Bell, E., & Burkert, A. 2006, ApJ, 638, 797
 Dobbs, C. L., Burkert, A. & Pringle, J. E. 2011a, MNRAS, 413, 2935
 Dobbs, C. L., Burkert, A. & Pringle, J. E. 2011b, MNRAS, 417, 1318
 Dobbs, C. L., Pringle, J. E., & Burkert, A. 2012, arXiv:1206.4904
 Elmegreen, B. G., & Elmegreen, D. M. 1978, ApJ, 220, 1051
 Evans, N. J., II, Dunham, M. M., Jørgensen, J. K., et al. 2009, ApJS, 181, 321
 Froebrich, D., & Rowles, J. 2010, MNRAS, 406, 1350
 Gao, Y., & Solomon, P. M. 2004, ApJ, 606, 271
 Goldsmith, P. F., Heyer, M., Narayanan, G., et al. 2008, ApJ, 680, 428
 Hartmann, L., Ballesteros-Paredes, J., & Bergin, E. A. 2001, ApJ, 562, 852
 Heiderman, A., Evans, N. J., II, Allen, L. E., Huard, T., & Heyer, M. 2010, ApJ, 723, 1019 (H10)
 Hennebelle, P., & Audit, E. 2007, A&A, 465, 431
 Heitsch, F., Slyz, A. D., Devriendt, J. E. G., Hartmann, L. W., & Burkert, A. 2007, ApJ, 665, 445
 Heitsch, F., Hartmann, L. W., Slyz, A. D., Devriendt, J. E. G., & Burkert, A. 2008, ApJ, 674, 316
 Heitsch, F., & Hartmann, L. 2008, ApJ, 689, 290
 Johnstone, D., Di Francesco, J., & Kirk, H. 2004, ApJ, 611, L45
 Kainulainen, J., Beuther, H., Henning, T., & Plume, R. 2009, A&A, 508, L35
 Kainulainen, J., Beuther, H., Banerjee, R., Federrath, C., & Henning, T. 2011, A&A, 530, A64
 Krumholz, M. R., Dekel, A. & McKee, C. F. 2012, ApJ, 745, 69
 Lada, E. A. 1992, ApJ, 393, L25
 Lada, E. A., Strom, K. M., & Myers, P. C. 1993, Protostars and Planets III, 245
 Lada, C. J., Lombardi, M., & Alves, J. F. 2010, ApJ, 724, 687
 Lada, C. J., Forbrich, J., Lombardi, M., & Alves, J. F. 2012, ApJ, 745, 190
 Mizuno, A., Onishi, T., Yonekura, Y., et al. 1995, ApJ, 445, L161
 Myers, P. C., & Benson, P. J. 1983, ApJ, 266, 309
 Onishi, T., Mizuno, A., Kawamura, A., Ogawa, H., & Fukui, Y. 1998, ApJ, 502, 296
 Ostriker, E. C., Stone, J. M., & Gammie, C. F. 2001, ApJ, 546, 980
 Pon, A., Johnstone, D., & Heitsch, F. 2011, ApJ, 740, 88
 Vázquez-Semadeni, E. 1994, ApJ, 423, 681
 Vázquez-Semadeni, E., Gómez, G. C., Jappsen, A. K., et al. 2007, ApJ, 657, 870
 Vázquez-Semadeni, E., Gómez, G. C., Jappsen, A.-K., Ballesteros-Paredes, J., & Klessen, R. S. 2009, ApJ, 707, 1023
 Wu, J., Evans, N. J., II, Shirley, Y. L., & Knez, C. 2010, ApJS, 188, 313
 Zamora-Avilés, M., Vázquez-Semadeni, E., & Colín, P. 2012, ApJ, 751, 77

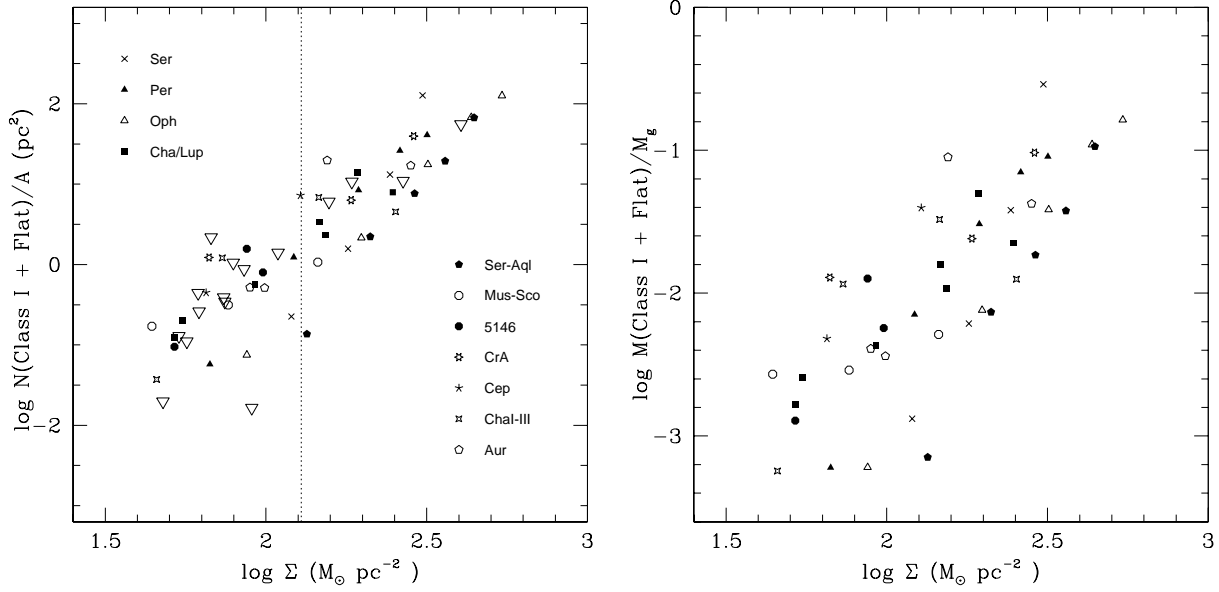


Figure 1. Left: The correlation of the number of protostars per unit area as a function of Σ , using the data of H10 (their Table 2). Differing symbols indicate differing clouds, labeled by the identifiers used by H10. Downward pointing large open triangles show “upper limits”, regions where no protostars were found, and so a value of one protostar was assigned for plotting purposes, as in H10. This is essentially the data plotted in Figure 8 of H10, except that we have not divided by a constant star-forming timescale of 2 Myr, we have added the number of Class I and flat-spectrum sources together, and did not include data from the HCN clumps (see text). Right: The total protostellar mass (as estimated from the total number of Class I and flat-spectrum sources, multiplied by an average mass of $0.7M_\odot$, and divided by the gas mass within the contour, as a function of Σ). Note that the slope is not significant because the quantities in both axes depend upon Σ (i.e., $M_g = \Sigma \times A(\Sigma)$). However, it is suggestive that, at high Σ , the ratio of stellar to gas mass begins to exceed 10% (see text)

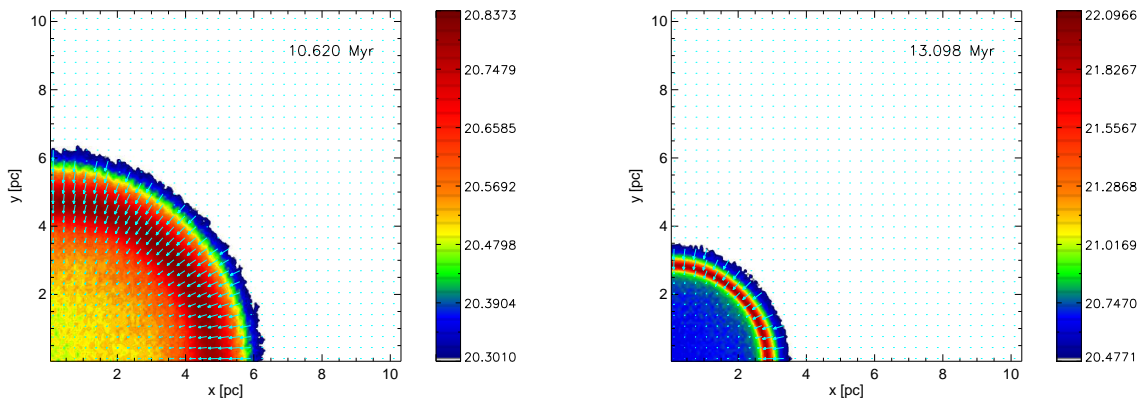


Figure 2. Evolution of the collapsing sheet (standard model). The surface density is plotted in logarithmic units of $N(H_2)$ (see text).

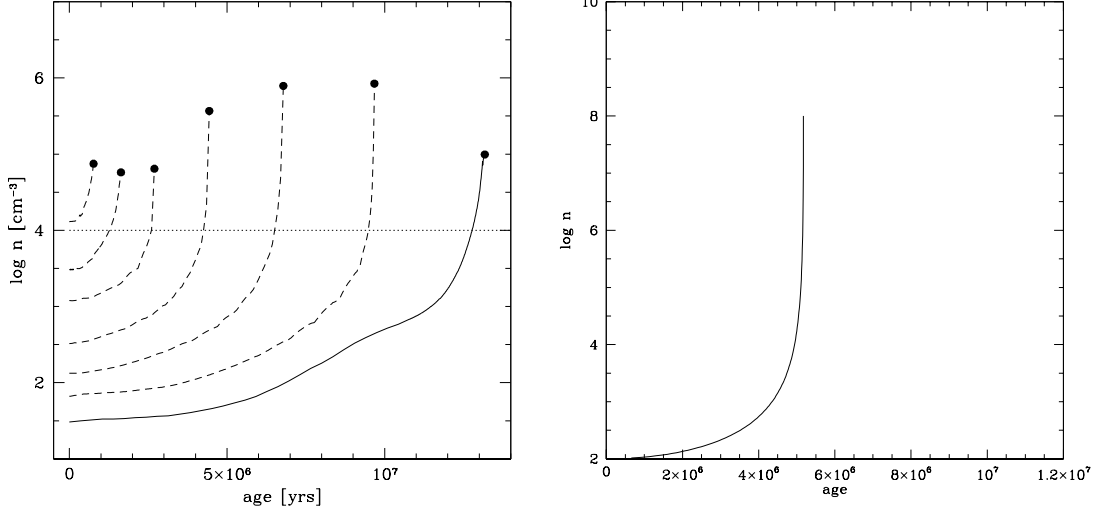


Figure 3. Left: Evolution of mean ring densities for the standard model with $M_c = 10^3 M_\odot$ (solid curve) and simulations with initial masses of 1.5×10^3 , 2×10^3 , 3×10^3 , 6×10^3 , 1×10^4 and $2 \times 10^4 M_\odot$. The filled points show the time when collapsing fragments appear in the ring. Right: evolution of density for the uniform free-falling sphere.

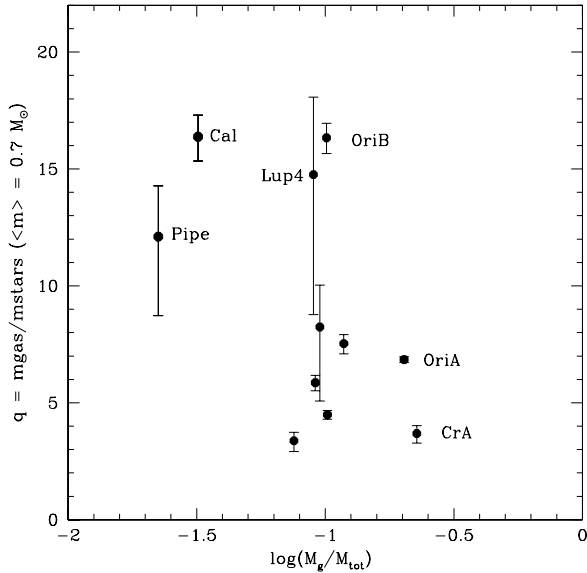


Figure 4. The ratio q of gas mass M_g above Σ_c to the estimated mass of young stars M_* , plotted as a function of the ratio of M_g to the total cloud mass, using data from Table 2 of L10. A mean mass of $0.7 M_\odot$ per star has been used to convert the number of stars to a total stellar mass. Errorbars reflect *only* counting statistics for the number of stars. There is an indication that q decreases as the fraction of dense gas mass increases (see text)

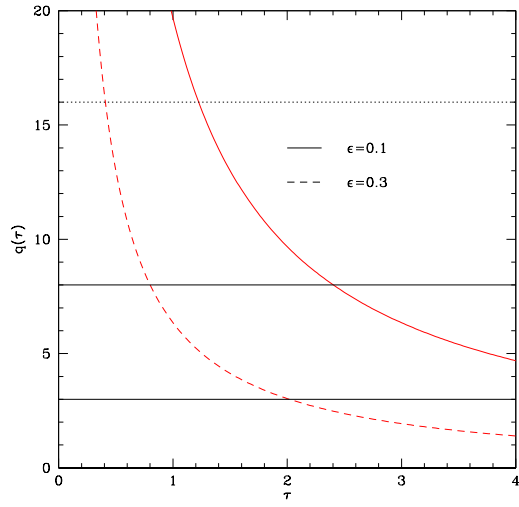


Figure 5. Results for the solution of equations 8 and 9, and adopting $M_{g,0} = 0$ for two values of ϵ . The dotted horizontal line indicates the observed upper q , while the two solid horizontal lines indicate the empirical limits for the “evolved clouds” (see text).

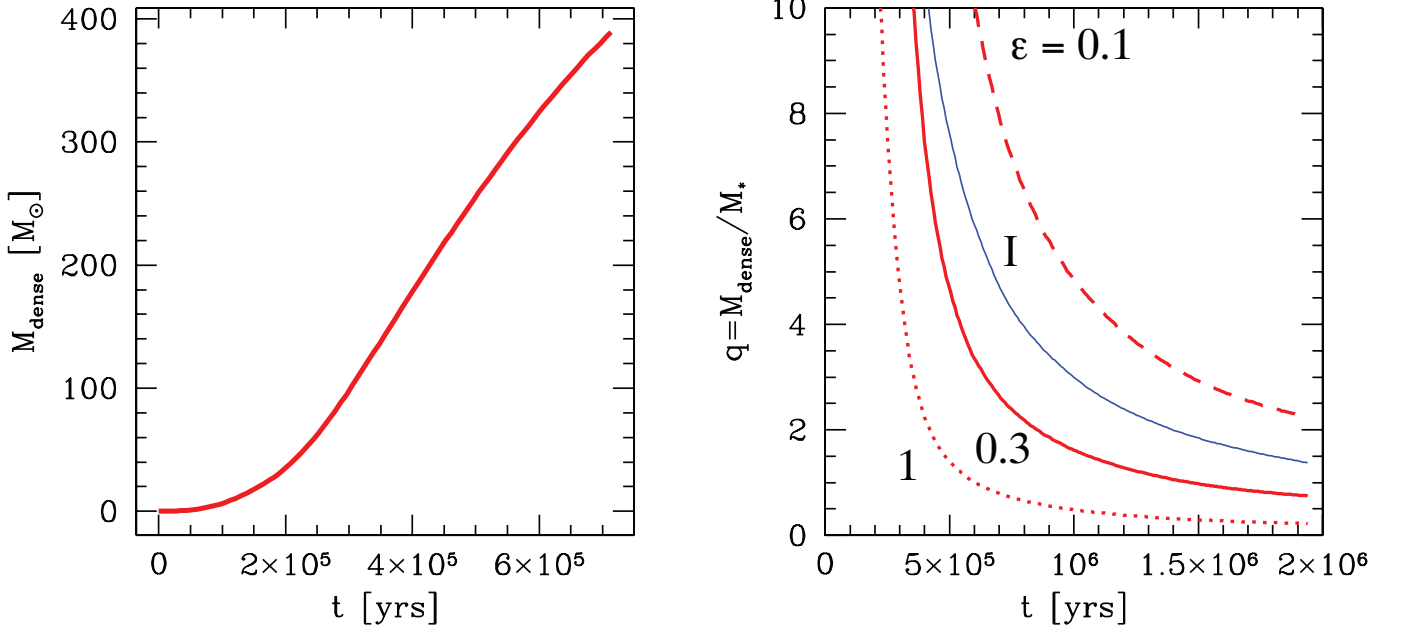


Figure 6. Inferred ratios of stars to dense gas, using the standard model simulation and various assumptions about star formation rates. On the left, the evolution of dense gas with a time offset. In the right panel, we show $q = M_g / M_*$ as a function of time assuming $M_g = M_{\text{dense}} - M_*$, where M_{dense} is the total gas as in the left-hand panel, and M_* the mass in the circular filament above that critical density 0.35 Myr earlier, times an efficiency factor ϵ . The dotted curve assumes $\epsilon = 1$, the solid red curve $\epsilon = 0.3$, and the dashed curve $\epsilon = 0.1$. The blue solid curve, labeled *I*, shows the situation assuming that after every 0.35 Myr a new, independent dense gas region forms that does exactly the same thing as the $\epsilon = 0.3$ case, just starting later (see text).

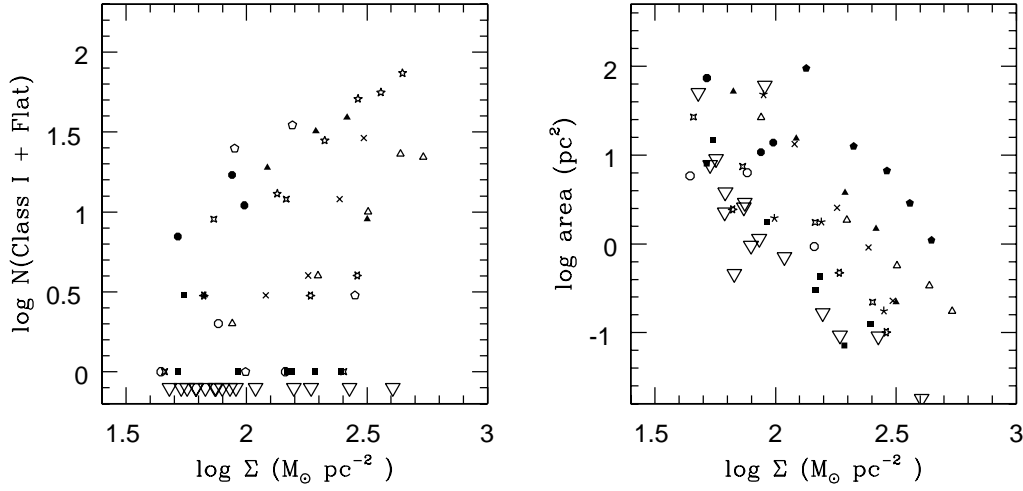


Figure 7. Left: relation between the number of protostars within a contour of area A as a function of Σ . The correlation is not strong, though individual regions (Ser-Aql, pentagons; Oph, open triangles; Cep, crosses; Per, filled triangles) show a trend of N increasing with Σ . The weak correlations are probably mostly due to the small number statistics, as evidenced by the contours containing zero protostars (downward-pointing open triangles). Right: area of each contour vs. Σ of that contour. There is a clear correlation; moreover, individual regions show similar slopes with vertical displacements. The results indicate that the correlation seen in Figure 1 is driven mainly by the $A(\Sigma)$ relation. Symbols as in Figures 1 and 8.

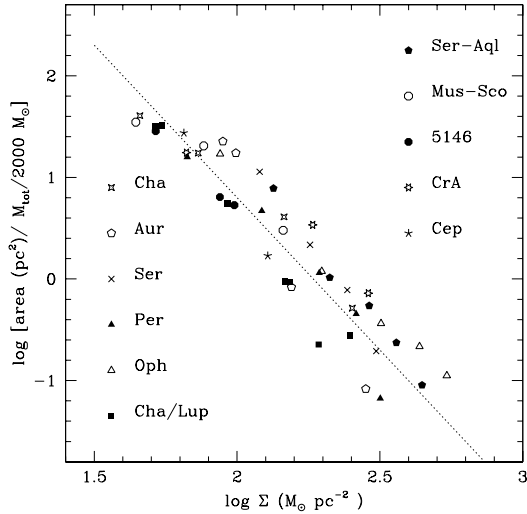


Figure 8. Areas at differing extinction contour levels, normalized by the scaled total cloud mass above an extinction threshold $A_V = 2$ (from Table 1 in H10) for the clouds in Table 2 of H10 with more than one young star contained within the contour. The dotted line shows the least square fit.